

Spectral properties of acoustic black hole radiation: Broadening the horizon

Stefano Finazzi*

SISSA, via Bonomea 265, Trieste 34151, Italy and INFN sezione di Trieste, Via Valerio 2, Trieste 34127, Italy

Renaud Parentani†

*Laboratoire de Physique Théorique, CNRS UMR 8627,
Bâtiment 210, Université Paris-Sud 11, 91405 Orsay Cedex, France*

(Dated: September 20, 2021)

The sensitivity of the black hole spectrum when introducing short distance dispersion is studied in the context of atomic Bose condensates. By considering flows characterized by several length scales, we show that, while the spectrum remains remarkably Planckian, the temperature is no longer fixed by the surface gravity. Rather it is determined by the average of the flow gradient across the horizon over an interval fixed by the healing length and the surface gravity, as if the horizon were broadened. This remains valid as long as the flow does not induce nonadiabatic effects that produce oscillations or some parametric amplification of the flux.

PACS numbers: 04.62.+v, 04.70.Dy, 03.75.Kk

I. INTRODUCTION

In the hydrodynamic approximation, i.e. for long wavelengths, the propagation of sound waves in a moving fluid that crosses the speed of sound is analogous to that of light in a black hole metric [1]. However, Hawking radiation relies on short wavelength modes [2–4]. Therefore the dispersion of sound waves must be taken into account when computing the spectrum emitted by an acoustic black hole. To this end, Unruh wrote a dispersive wave equation in a supersonic flow [5]. Through a numerical analysis, he then showed that the spectrum was robust, provided the dispersive scale ξ , the “healing length”, is much smaller than the surface gravity scale $1/\kappa$ which fixes the Hawking temperature $T_H = \kappa/2\pi$ (in units where $\hbar = k_B = c = 1$). This insensitivity was then confirmed by analytical [6–9] and numerical [10–13] methods. However it turned out that the *deviations* with respect to the standard flux are much harder to characterize, and so far there is no consensus on what are the relevant parameters.

To address this question, we consider velocity profiles characterized by several scales, and numerically compute the spectrum by varying them separately. Whenever $\omega_{\max}/T_B \gtrsim 10$, where ω_{\max} is a critical frequency [12, 13] that scales with $1/\xi$ but also depends on the asymptotic flow velocity, the flux remains Planckian to a high accuracy, *even* when the temperature completely differs from T_H . In fact, we show that the temperature is determined by the average of the velocity gradient across the horizon over a critical length fixed by ξ and κ . In [14], we analytically explain the origin of that length.

These properties hold for large classes of flows. They cease to be valid only if the flow induces nonadiabatic

effects that interfere with the Hawking effect, thereby introducing oscillations in the spectrum. This is illustrated by considering *undulations* similar to those appearing in white holes’ flows [15, 16]. For definiteness we use the Bogoliubov–de Gennes (BdG) equation in the context of atomic Bose condensates. However our results apply to other analogue models, e.g. with subluminal dispersion relations, and, more generally, to all dispersive theories.

We have organized the paper as follows. We first present the multiparameter flow profiles we shall use. We then analyze the phonon spectrum obtained by numerically solving the mode equation. In Appendixes we briefly present the concepts which are needed to obtain the phonon flux, starting from the BdG equation.

II. CHOICE OF FLOW PROFILES

In this paper we consider elongated condensates that are stationary flowing along the longitudinal direction x . We also assume that the transverse dimensions are small enough that relevant phonon excitations are longitudinal. In that case, one effectively deals with a 1+1 dimensional field. Then, using the analogy [1, 17] between sound propagation in the hydrodynamic regime and light, the flow defines a metric of the form

$$ds^2 = -c^2 dt^2 + (dx - v dt)^2, \quad (1)$$

where v is the flow velocity and c the speed of sound. For stationary flows, c and v only depend on x . Assuming that the condensate flows from right to left ($v < 0$), a sonic horizon is present where $w = c + v$ crosses 0. It corresponds to a black hole horizon when $\partial_x w > 0$, and a white one when $\partial_x w < 0$. We shall call it a Killing horizon since the norm of the Killing field ∂_t vanishes when $w = 0$ [17]. Its location is taken at $x = 0$.

When ignoring short distance dispersion, the spectrum of the upstream phonons spontaneously emitted from a black hole horizon is simple, and strictly corresponds to

*Electronic address: finazzi@sissa.it

†Electronic address: renaud.parentani@th.u-psud.fr

the Hawking radiation [1, 5]. It follows a Planck law and the temperature is fixed by the decay rate¹

$$\kappa_K \equiv \partial_x(c+v)|_{x=0}. \quad (2)$$

For relativistic fields indeed, κ_K gives the late time decay rate of the frequency of outgoing modes, as seen by asymptotic observers, see Eq. (32.8) in [19] for classical waves, and Eq. (3.44) in [4] for Hawking radiation. As a result, κ_K fixes the temperature to be exactly $T_H = \kappa_K/2\pi$, in units where $\hbar = k_B = 1$, but independently of c_0 , the value of the sound speed at the horizon.

When including dispersion, these results are no longer true because the total amount of redshift saturates. Nevertheless, the κ_K -decay law is recovered near the horizon where $w = c+v$ is linear in x . Moreover, when the healing length is much smaller than c_0/κ_K , this guarantees that the spectrum and the correlations of the Hawking pairs are not significantly affected by dispersion [6, 20, 21].

As already mentioned, the difficulties start when one tries to characterize the deviations from the Planck spectrum at temperature T_H . This is because these have different origin and are governed by different parameters. In spite of this, we shall see that they can be analyzed and understood. To this end, we shall work with flow profiles governed by *several* scales, and of the form

$$c(x) + v(x) = w(x) = w_B(x) + w_p(x), \quad (3)$$

where w_B is a reference background profile and w_p a perturbation of smaller amplitude: $0 \leq |w_p(x)| \lesssim |w_B(x)|$. The metric (1) is then completely fixed by introducing q ,

$$\begin{aligned} c(x) &= c_0 + (1-q)w(x), \\ v(x) &= -c_0 + qw(x), \end{aligned} \quad (4)$$

which specifies how $c+v$ is shared between c and v . In all simulations, we work with $q = 1/2$, because it minimizes the scattering between left and right moving phonons which is not related to the Hawking effect (see Fig. 11 in [13]). Hence working with $q = 1/2$ will ease the identification of the other, more intrinsic, deviations with respect to the standard flux. Similarly, to have well-defined asymptotic modes, we work with infinite condensates and with c, v possessing well-defined values for $x \rightarrow \pm\infty$.

The background profile is given by

$$\frac{w_B(x)}{c_0} = D \times \text{sign}(x) \left[\tanh \left\{ \left(\frac{\kappa_B |x|}{c_0 D} \right)^n \right\} \right]^{1/n}. \quad (5)$$

The quantity D fixes the asymptotic value of w_B , whereas n governs the smoothness of the transition from the region where w_B is linear in x to the asymptotic regime

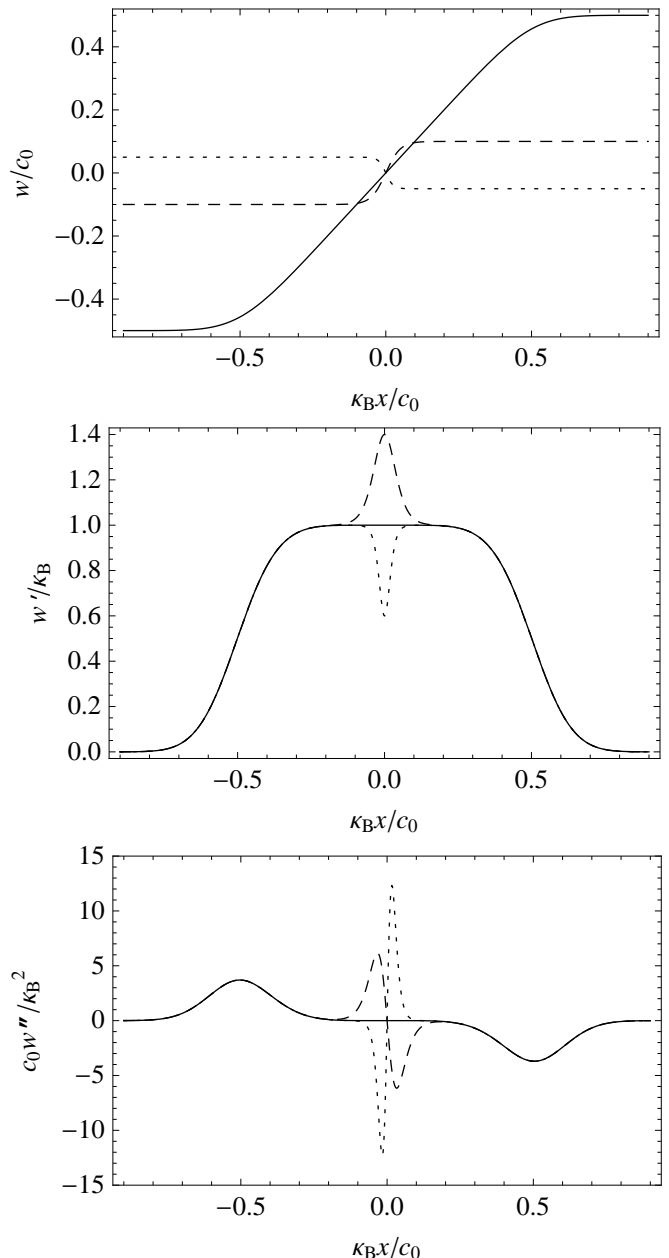


FIG. 1: Upper panel: background flow w_B (solid line) for $n = 3$, $D = 0.5$ and two perturbations w_p (amplified by a factor of 5, dashed and dotted lines), with $n_p = 1$, and $(\kappa_p/\kappa_B, D_p)$ equal to $(0.4, 0.02)$ and $(-0.4, 0.01)$. Central and lower panel: first and second derivative of w_B (solid line) and of $w = w_B + w_p$ (dashed and dotted lines) for the same w_p . Narrower perturbations induce higher modifications of derivatives of w .

where it is constant. We shall work with $n = 1$ or 2 to have a well-defined range $\sim c_0 D/\kappa_B$ where w_B is linear, and yet avoid the nonadiabatic effects [10, 12] when the transition is too sharp, i.e., when $n \geq 4$.

We shall consider two types of perturbations, symmetric ones with respect to the horizon, i.e., $w_p(x) = -w_p(-x)$, and then, in Sec. IV, more general ones with-

¹ To adopt the standard terminology, we shall call κ_K the *surface gravity* [18], even though the latter has a dimension of an acceleration, and has no clear physical meaning for sound waves.

out that symmetry. The symmetric ones are similar to w_B :

$$\frac{w_p(x)}{c_0} = D_p \times \text{sign}(x) \left[\tanh \left\{ \left(\frac{\kappa_p |x|}{c_0 D_p} \right)^{n_p} \right\} \right]^{1/n_p}. \quad (6)$$

The condition $0 \leq |w_p| \lesssim |w_B|$ is simply $0 \leq D_p \lesssim D$. In Fig. 1, we plot $w(x)$, its first and second derivatives for different values of κ_p/κ_B and D_p .

The smoothness parameter n_p will range from 0.5 to 4. We shall see that it only affects the flux marginally. In fact the most important quantity is D_p . Its role is to fix

$$|x_{\text{lin}}| \sim \frac{c_0 D_p}{\kappa_p}, \quad (7)$$

the interval of x over which $w(x)$ is linear. In this respect, it should be noticed that the surface gravity is equal to

$$\kappa_K \equiv \partial_x(c+v)|_{x=0} = \kappa_B + \kappa_p, \quad (8)$$

irrespective of the value of D_p , and that of n_p . For relativistic fields, D_p would play no role since the temperature is $\kappa_K/2\pi$ (when ignoring gray body factors, a correct approximation in our settings when $q = 1/2$). For dispersive fields instead, D_p plays a crucial role.

III. SPECTRAL ANALYSIS

In a stationary condensate flowing with a velocity v , the dispersion relation of phonons is given by [22]

$$(\omega - vk)^2 = \Omega^2(k) = c^2 k^2 + \frac{\hbar^2 k^4}{4m^2} = c^2 k^2 + \frac{c^4 k^4}{\Lambda^2}, \quad (9)$$

where ω is the conserved frequency ∂_t , m the atom mass, and Λ the frequency associated with the healing length $\xi = \hbar/\sqrt{2}mc$ by $\Lambda = \sqrt{2}c/\xi$.

In what follows we study the properties of n_ω , the mean occupation number of phonons of frequency ω spontaneously emitted to the right region, i.e. against the flow, when the initial state is vacuum. In order to focus on new results, we have decided to present in the Appendixes a summary of the concepts needed to compute n_ω , starting from the BdG equation applied to the flows of Eq. (3). The figures of this paper have been obtained by numerically solving Eq. (B6) with the code of Ref. [13].

Our program can now be clearly defined: we shall study n_ω in the perturbed flows for increasing D_p to see how the phonon field “responds” to the introduction of w_p . We start with the symmetrical profiles of Eq. (6), and then consider asymmetrical ones. The spectrum in the unperturbed flow of Eq. (5) has been studied in [10, 12, 13].

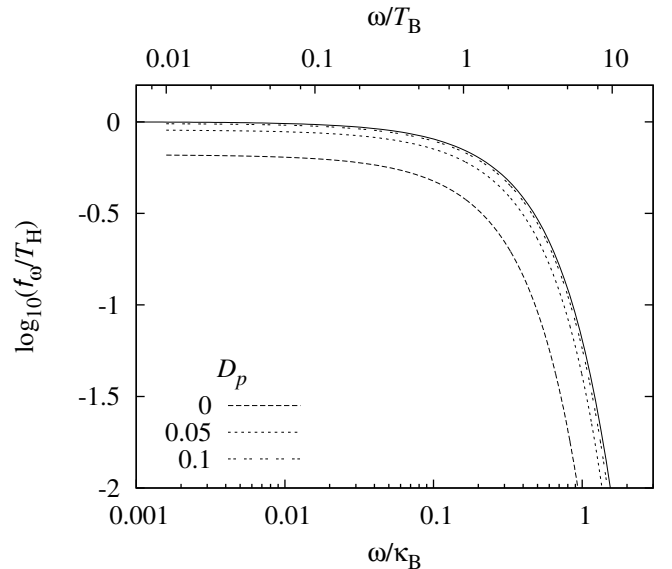


FIG. 2: $\log_{10}(f_\omega/T_H)$ versus ω/κ_B for different values of D_p , but the same surface gravity κ_K . The solid line represents the Planck flux at temperature $T_H = \kappa_K/2\pi$. When $D_p = 0.1$, the phonon flux hardly differs from it. For smaller values of D_p , the flux is weaker, and for $D_p \rightarrow 0$, it is fixed by the background surface gravity κ_B . The fixed parameters are $\Lambda/\kappa_B = 15$, $D = 0.4$, $\kappa_p/\kappa_B = 0.5$, $n = n_p = 1$.

A. Planckian character

In Fig. 2 we present the energy flux

$$f_\omega = \omega n_\omega, \quad (10)$$

as a function of ω for different values of the amplitude D_p , keeping fixed all the other parameters. When working with a relativistic massless field, one would obtain a Planck spectrum with a temperature $T_H = \kappa_K/2\pi$, irrespective of the value of D_p . To ease the comparison with the dispersive fluxes, we have represented this flux by a solid line. Working with the BdG equation (B6), we see instead that the flux varies with D_p . In fact it increases monotonically. Moreover, when $D_p \rightarrow 0$, we verified that it coincides with the flux one would obtain in the reference flow w_B . We also see that when D_p is sufficiently large, the flux saturates and agrees to a high accuracy with the Planck spectrum at temperature T_H , in accordance with the *robustness* [5, 6, 10] of the flux.

Since comparing energy fluxes f_ω is not convenient, we shall use the temperature function defined by

$$n_\omega \equiv \frac{1}{\exp(\omega/T_\omega) - 1}. \quad (11)$$

As such, T_ω is simply another way to express n_ω . However it presents the great advantage of being constant whenever the flux is Planckian.

In fact, as can be seen in Fig. 3, for *all* values of D_p , T_ω remains remarkably constant, until ω approaches the

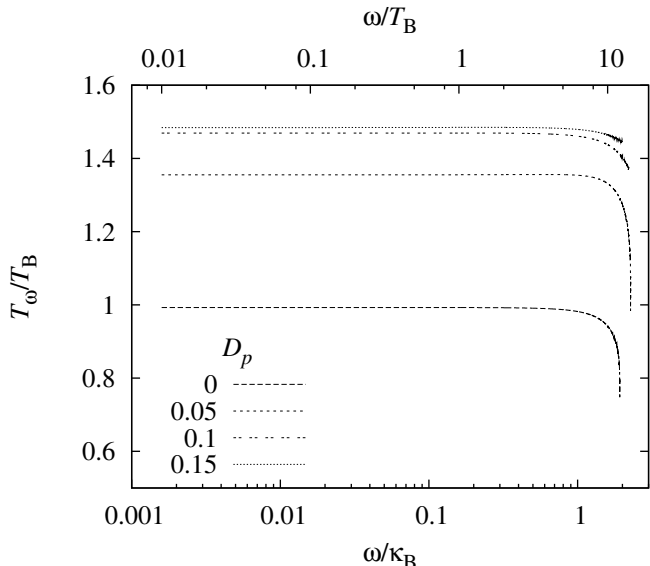


FIG. 3: T_ω/T_B of Eq. (11) versus ω/κ_B for various D_p but the same value of $\kappa_K = 1.5\kappa_B$. $T_B = \kappa_B/2\pi$ is the Hawking temperature of the background flow. The values of the parameters are those of Fig. 2. For all values of D_p , T_ω hardly varies until $\omega \rightarrow \omega_{\max}$ of Eq. (A3), where the flux vanishes. Since $\omega_{\max} \gtrsim 10 T_B$, as can be seen from the horizontal upper scale, these spectra are, to a high precision, Planckian.

critical frequency ω_{\max} of Eq. (A3). At that frequency, the signal drops down as it must do, since the Bogoliubov transformation (B8) becomes trivial, because the negative norm mode $\varphi_{-\omega}$ no longer exists above ω_{\max} . This cutoff effect relies on the asymptotic value of the flow $v + c$, and has been studied in detail in [12, 13]. In what follows we focus instead on the deviations of the spectrum which depend on the near horizon properties of $v + c$.

To quantify the small deviations from a Planck spectrum at temperature

$$T_0 \equiv \lim_{\omega \rightarrow 0} T_\omega, \quad (12)$$

we studied the relative deviation

$$\Delta_T(\omega) \equiv \frac{T_0 - T_\omega}{T_0}. \quad (13)$$

evaluated for $\omega = T_0$. For all values of D_p we found

$$|\Delta_T(T_0)| \lesssim 3. \times 10^{-4}. \quad (14)$$

We note that $\Delta_T(T_0) \neq 0$ is not due to numerical errors, it really characterizes the deviations.

Equation (14) implies that, to a high accuracy, the spectrum remains Planckian even when T_0 completely differs from T_H . (In the present case, it differs by 33%, since $\kappa_K = 1.5\kappa_B$.) The smallness of $\Delta_T(T_0)$ also implies that the parameters that govern the deviations from Planckianity *differ* from those governing the shift $T_0 - T_H$.

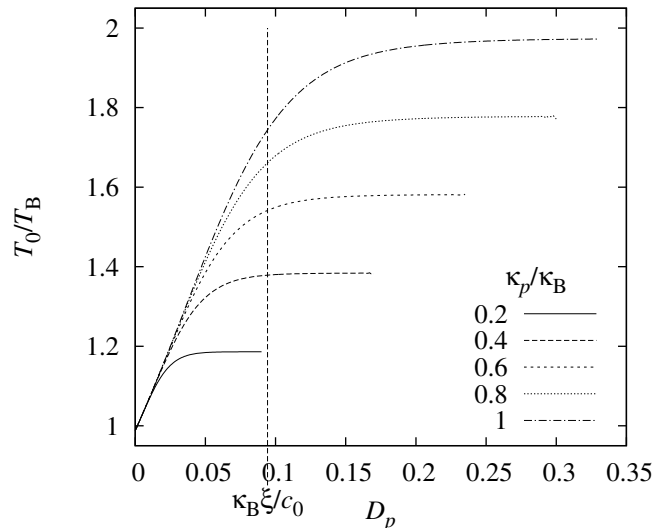


FIG. 4: T_0/T_B versus D_p for κ_p/κ_B from 0.2 to 1, and with $\Lambda/\kappa_B = 15$, $D = 0.3$, $n = n_p = 1$. Along each curve the surface gravity κ_K of Eq. (8) is *constant*. It fixes the temperature *only* for $D \gg D_p^{\text{crit}}$. The vertical line gives the value of the healing length ξ .

Hence when studying the robustness of the Hawking flux against introducing dispersion, one must differentiate these two types of deviations.

These are our first important results. They generalize what was observed in [12, 13] to a much wider class of flows, namely, first, that the thermality is well preserved whenever $\omega_{\max}/T_B \gtrsim 10$, and, second, that the relative temperature shift $T_0/T_H - 1$ is much larger than $\Delta_T(T_0)$. In the sequel we work with $\omega_{\max}/T_B \gtrsim 10$ satisfied, and study how the low frequency temperature T_0 depends on κ_p , D_p , n_p and Λ .

B. The critical value of D_p

In Fig. 3, we saw that T_0 starts from $\kappa_B/2\pi$ for $D_p \rightarrow 0$, and asymptotes to $T_H = \kappa_K/2\pi$ for D_p larger than some critical value D_p^{crit} . (We have checked that this is also the case when $\kappa_p < 0$, and this down to $\kappa_p = -\kappa_B$, in which case the surface gravity κ_K vanishes.) To understand what fixes D_p^{crit} , we first consider series of flows $w_B + w_p(D_p)$ for different values of κ_p at fixed κ_B . For each series, the surface gravity $\kappa_K = \kappa_B + \kappa_p$ is thus constant. The resulting temperatures $T_0(D_p)$ are presented in Fig. 4. This figure reveals many interesting features. For small values of D_p , T_0 increases linearly with D_p in a manner essentially *independent* of κ_p . In addition, for each series, when D_p is large enough, T_0 saturates at the standard result $T_H = \kappa_K/2\pi$.

Given the linear behavior of T_0 for small D_p and the

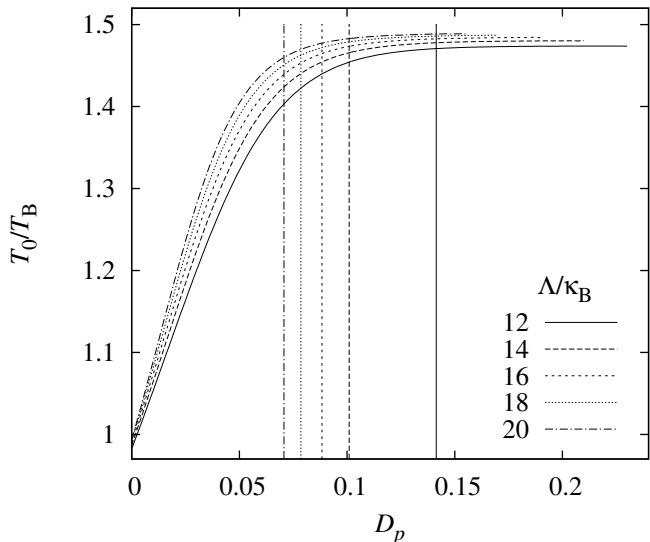


FIG. 5: T_0/T_B versus D_p for Λ/κ_B from 12 to 20, and with $\kappa_p/\kappa_B = 0.5$, $D = 0.3$, $n = n_p = 1$. The vertical lines give the values of the healing length $\xi = \sqrt{2}c_0/\Lambda$. One can see that D_p^{crit} of Eq. (17) is *not* (directly) related to ξ .

saturation for large values, i.e.,

$$\begin{aligned} 2\pi T_0(D_p \ll D_p^{\text{crit}}) &\sim \kappa_B + s D_p, \\ 2\pi T_0(D_p \gg D_p^{\text{crit}}) &\sim \kappa_B + \kappa_p = \kappa_K, \end{aligned} \quad (15)$$

we define D_p^{crit} as the value of D_p where these intercept, and obtain

$$D_p^{\text{crit}} = \frac{\kappa_p}{s}. \quad (16)$$

To understand what fixes the slope s , we consider series of flows with different values of the ultraviolet dispersion scale Λ . The results are presented in Fig. 5. It is numerically easy to see that $s \propto \Lambda^{2/3}$. Hence we get

$$D_p^{\text{crit}} \propto \kappa_p \Lambda^{-2/3}. \quad (17)$$

We now present a simple argument telling how D_p^{crit} should scale with the various parameters. In [13], by considering w_B of Eq. (5), it was *observed* that the leading deviations due to dispersion are governed by inverse powers of $\omega_{\text{max}}/\kappa_B$. For these unperturbed flows, ω_{max} of Eq. (A3), even though initially defined as the frequency such that the turning point $x_{\text{tp}}(\omega)$ of Eq. (A2) is rejected at $-\infty$, also corresponds to the frequency such that the turning point is at the edge of the domain $\sim c_0 D/\kappa_B$, where w_B is linear in x .

When working with $w = w_B + w_p$ of Eq. (6) and with $D_p \ll D$, the linear domain is now given by x_{lin} of Eq. (7). Hence we expect that the deviations will be now governed by inverse powers of $\omega_{\text{Mp}}/\kappa_K$, where ω_{Mp} is the new critical frequency fixed by x_{lin} . The value of

ω_{Mp} is such that the turning point $|x_{\text{tp}}(\omega)|$ of Eq. (A2) equals x_{lin} . Using Eq. (7), $|x^{\text{tp}}(\omega_{\text{Mp}})| = x_{\text{lin}}$ gives

$$\omega_{\text{Mp}} = \Lambda \left(\frac{\kappa_K}{\kappa_p} D_p \right)^{3/2}. \quad (18)$$

Since the deviations from the standard result should be small when $\omega_{\text{Mp}}/\kappa_K \gg 1$, D_p^{crit} should scale as

$$D_p^{\text{crit}} \propto \frac{\kappa_p}{(\kappa_K \Lambda^2)^{1/3}}. \quad (19)$$

A rigorous study [14] of the connection formulas [6–9] confirms the result of this simple reasoning.

Equation (19) is in agreement with Eq. (17) for $\kappa_p \ll \kappa_B$. In the following section, we shall numerically validate it for all values of κ_p . Before proceeding, we checked that D_p^{crit} does not significantly depend on the background quantities n , D and κ_B , as one could have expected. The weak, subleading, dependence on n_p is studied in Sec. III D.

C. The averaged surface gravity

So far we have some understanding of the Planckian character of the flux in the robust regime when $D_p > D_p^{\text{crit}}$, and of the value of D_p^{crit} [14]. Instead, what fixes T_ω outside this regime, for $D_p < D_p^{\text{crit}}$, is *terra incognita*.

We shall now numerically establish that, to a good approximation when $\omega_{\text{max}}/T_B \gtrsim 10$, the temperature is determined by the average of the gradient dw/dx over a width that we parametrize by $d_\xi = d_\xi^L + d_\xi^R$, where d_ξ^L and d_ξ^R are respectively the width on the left and on the right calculated from the Killing horizon at $x = 0$.

In fact, given that the dispersion of Eq. (9) defines a ‘healing length’ $\xi = \sqrt{2}c/\Lambda$, it is not surprising that ξ in turns defines a minimal resolution length, such that details of $w(x)$ smaller than d_ξ are not “seen” by the phonon field. In other words, because of dispersion, it is as if we were dealing with a horizon of width d_ξ .² Moreover, when $d_\xi^L \neq d_\xi^R$, this means that the center of the effective horizon is *displaced* with respect to the Killing horizon to $\bar{x}_{\text{hor}} = (d_\xi^R - d_\xi^L)/2$.

To test the idea that the temperature be determined by an average “surface gravity,” we introduce

$$\bar{\kappa} \equiv \frac{1}{d_\xi} \int_{-d_\xi^L}^{d_\xi^R} dx \frac{dw(x)}{dx} = \frac{w(d_\xi^R) - w(-d_\xi^L)}{d_\xi}. \quad (20)$$

² This important result should be opposed to the possibility discussed in [9, 23] according to which T_ω could be governed by a local, ω -dependent, function of w , e.g. by the value of $\partial_x w$ evaluated at the turning point of Eq. (A2). In fact our numerical results indicate that it is a *non-local* quantity that fixes the temperature, and in a manner essentially independent of ω . This is in sympathy with the ideas that quantum gravitational effects might blur the horizon [24, 25] and that dispersion might regulate the black hole entanglement entropy [26].

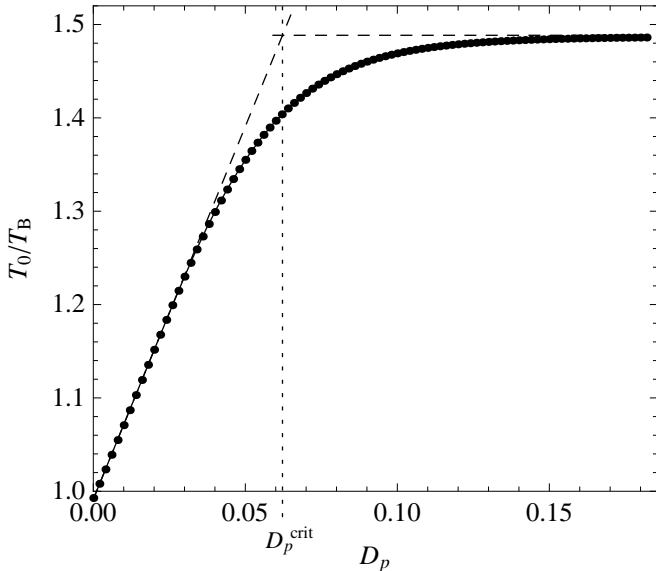


FIG. 6: Dots: T_0/T_B versus D_p computed for $\Lambda/\kappa_B = 15$, $D = 0.4$, $n_p = n = 1$, $\kappa_p/\kappa_B = 0.5$. Solid line: best fit curve obtained by using $\bar{\kappa}/2\pi$ of Eq. (21). The perfect agreement establishes that the temperature T_0 equals $\bar{\kappa}/2\pi$. Dashed lines: asymptotic behaviors for $D_p \ll D_p^{\text{crit}}$ and $D_p \gg D_p^{\text{crit}}$ [see Eqs. (15) and (16)].

Using Eqs. (5) and (6), we get

$$\bar{\kappa} = \kappa_B + \frac{w_p(d_\xi^R) + w_p(d_\xi^L)}{d_\xi} + O\left[\left(\frac{\kappa_B d_\xi}{D c_0}\right)^{2n}\right], \quad (21)$$

where we assume that $d_\xi \ll D/\kappa_B$, so that the average of the background term w_B is approximately κ_B .

We proceed as follows: We compute T_0 for about 200 values of D_p for some fixed values of the perturbed flow parameters (n_p, κ_p) and the dispersive scale Λ , i.e., along series as those represented in Figs. 4 and 5. Out of this set we extract five quantities, namely, $\kappa_B^{(\text{fit})}$, $n_p^{(\text{fit})}$, $\kappa_p^{(\text{fit})}$, d_ξ^L , and d_ξ^R , by fitting $\bar{\kappa}(\kappa_B, n_p, \kappa_p, d_\xi^L, d_\xi^R; D_p)/2\pi$ of Eq. (21) with a nonlinear least-squares method. The agreement between the couples $T_0(D_p)$ and the fitted function $\bar{\kappa}(D_p)/2\pi$ is really striking—see Fig. 6 for an example.

Moreover, the fitted values $\kappa_B^{(\text{fit})}$ and $\kappa_p^{(\text{fit})}$ are in very good agreement (less than 1.5% and 1%, respectively) with their values used in the flow w . This is a necessary check to validate that it is the average of $\partial_x w$ that governs the temperature. However, the agreement between $n_p^{(\text{fit})}$ and n_p is less good. This indicates that the actual temperature is not *exactly* given by the average of Eq. (20).³ Even though this is a subdominant

effect, it is interesting to see under which conditions a better agreement between $n_p^{(\text{fit})}$ and n_p is reached.

D. Subleading effects in n_p

The parameter n_p of Eq. (6) determines the smoothness of the transition between the region where $w_p(x)$ is linear, with constant derivative κ_p , and the region where it is flat, equal to $D_p c_0$. Larger values of n_p make that transition sharper. Therefore higher derivatives of w will become very large at the end of the linear-regime region, near x_{lin} of Eq. (7). As a consequence, nonadiabatic effects become more important, thereby generating larger deviations between T_0 and $\bar{\kappa}/2\pi$ of Eq. (21).

To investigate these deviations, we compare $T_0(D_p)$ for various values of n_p . As it appears from Fig. 7, left panel, s and D_p^{crit} do not significantly depend on n_p . However, the transition region between the linear regime and the constant regime depends on n_p . The transition is indeed monotonic for small values of n_p whereas, for $n_p > 1$, T_0 oscillates around $T_H = \kappa_K/2\pi$. The monotonic function of Eq. (20) will of course never describe these oscillations. However, for $n_p \leq 1$, one can compare $n_p^{(\text{fit})}$ with n_p . The result is shown in Fig. 7, right panel. The dots and the squares are computed using different values of Λ/κ_B , respectively 15 and 20. One sees that $n_p^{(\text{fit})}$ is always larger than n_p . One also sees that the discrepancy becomes smaller when n_p decreases, as expected, since nonadiabatic effects are smaller for smoother profiles, hence smaller n_p . One should not overestimate the relevance of this discrepancy because we found that the value of $n_p^{(\text{fit})}$ is correlated in the fitting procedure to the difference $d_\xi^R - d_\xi^L$. For instance, when imposing $d_\xi^R = d_\xi^L$, $n_p^{(\text{fit})} - n_p$ is reduced by a factor of about 2.

The important conclusion is the following. When nonadiabatic effects are small, the temperature of the phonon flux is well approximated by $1/2\pi$ times the average of $\partial_x w$ over a certain width d_ξ [see Eq. (20)].

E. The scaling laws of the width d_ξ

Unlike $\kappa_B, \kappa_p, n_p, D_p$ which characterize the flow w and Λ which fixes the healing length, d_ξ is not a parameter entering the mode equation (B6). Therefore the value obtained in a fit cannot be compared with some a priori known value. In fact d_ξ should be conceived as an *emergent*, effective, length scale.

Before using numerical results to determine how it scales when changing κ_K, κ_p and Λ , we point out that

slightly different results. At this point, we are not in the position to distinguish them. What is important is that the scaling laws we shall derive in Sec. III E are independent of the particular choice.

³ We notice that different averaging procedures could have been considered in the place of Eq. (20), and they would have given

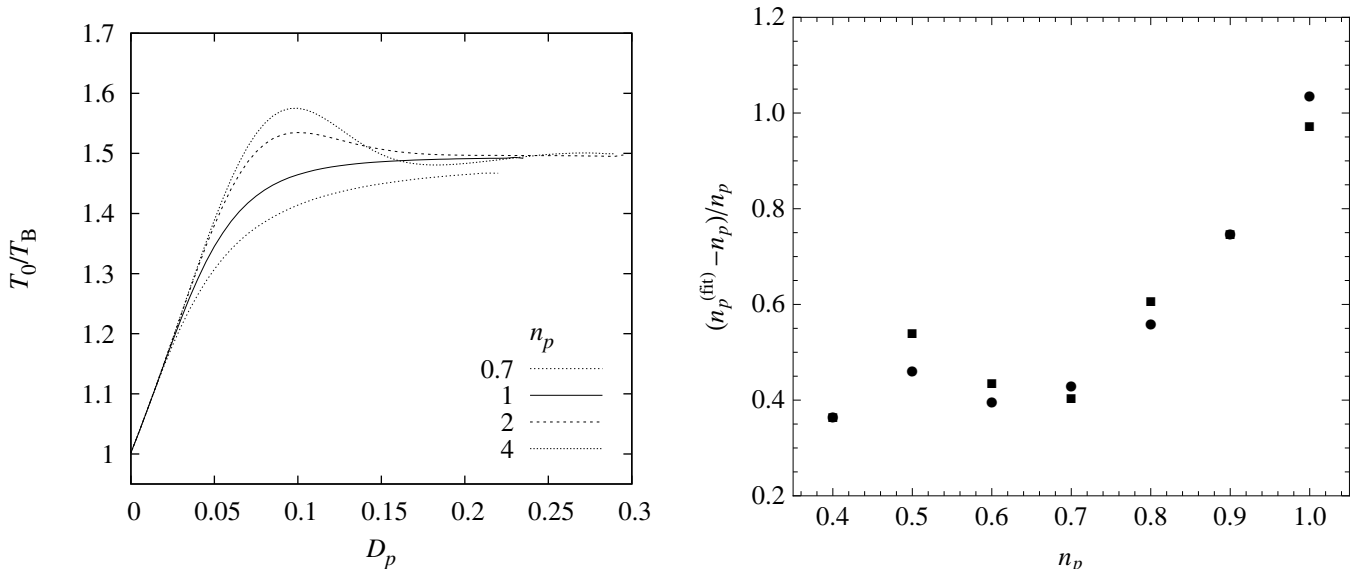


FIG. 7: Left panel: T_0/T_B versus D_p for different values of n_p of Eq. (6) with $\kappa_p/\kappa_B = 0.5$, $D = 0.4$, $n = 2$. T_0 monotonically approaches T_H for $n_p \leq 1$. When $n_p > 1$ instead, it exceeds T_H near D_p^{crit} and then approaches it with oscillations. Right panel: the relative difference $(n_p^{(\text{fit})} - n_p)/n_p$ versus n_p . The difference decreases for smaller n_p , in a rather insensitive way with respect to Λ/κ_B (dots, $\Lambda/\kappa_B = 15$; squares, $\Lambda/\kappa_B = 20$).

we can predict how it should do, as d_ξ is closely related to D_p^{crit} of Eq. (19). Indeed, taking the limits of Eq. (21) for small and large D_p we obtain

$$\begin{aligned} \bar{\kappa}(D_p \ll \frac{\kappa_p d_\xi}{c_0}) &\sim \kappa_B + \frac{2D_p c_0}{d_\xi}, \\ \bar{\kappa}(D_p \gg \frac{\kappa_p d_\xi}{c_0}) &\sim \kappa_K, \end{aligned} \quad (22)$$

and hence, using Eq. (15) and (16), we get

$$d_\xi = \frac{2c_0 D_p^{\text{crit}}}{\kappa_p}. \quad (23)$$

In other words, the critical value of D_p separating the two regimes of $T_0(D_p)$ shown in Fig. 6 strictly corresponds to the width d_ξ one should use in Eq. (20) to follow $T_0(D_p)$. Using Eq. (19), we get

$$d_\xi = d \times \frac{c_0}{(\kappa_K \Lambda^2)^{1/3}}, \quad (24)$$

where d is a constant. In terms of the healing length $\xi = \sqrt{2c_0}/\Lambda$, this gives

$$\frac{d_\xi}{\xi} = d \times \left(\frac{2\xi}{d_K} \right)^{-1/3}, \quad (25)$$

where $d_K \equiv c_0/\kappa_K$ is the surface gravity length. Hence, when $\xi \ll d_K$, d_ξ is significantly larger than ξ .

The prediction of Eq. (24) can be numerically validated

by a linear ⁴ least-square fit of

$$\begin{aligned} \log(d_\xi \frac{\kappa_B}{c_0}) &= \log(d) + a \log\left(\frac{\Lambda}{\kappa_B}\right) + b \log\left(\frac{\kappa_p}{\kappa_B}\right) \\ &\quad + c \log\left(1 + \frac{\kappa_p}{\kappa_B}\right). \end{aligned} \quad (26)$$

We used a grid of 110 values of (κ_p, Λ) . The corresponding values of $d_\xi(\kappa_p, \Lambda)$ are extracted from series of about 200 couples (T_0, D_p) using the procedure described after Eq. (20). κ_p/κ_B ranges from 0.1 to 1, with step 0.1 and Λ/κ_B ranges from 10 to 20 with unitary step. The other parameters are $D = 0.4$, $n = n_p = 1$, $q = 0.5$.⁵

The result of the fit is

$$\begin{aligned} a &= -0.627, & b &= 0.024, \\ c &= -0.33, & d &= 1.58, \end{aligned} \quad (27)$$

where the numerical error is on the last figure. The exponent a differs from about 5% from its expected value

⁴ When the function is linear in the parameters, a close-form solution of the χ^2 minimization problem is available. This method is therefore preferable to non-linear ones.

⁵ Because of numerical noise, for some series (Λ, κ_p) , it was not possible to obtain a sufficiently large number of points (T_0, D_p) . In particular it is difficult to obtain T_0 for large values of D_p . We therefore decided to use only the series for which we obtain T_0 for every value of D_p from 0 to 0.1 (namely 100 points, with step 0.001). In this way, there are points with $D_p \gtrsim D_p^{\text{crit}}$ in the series (T_0, D_p) used to determine d_ξ . This condition is satisfied by 71 series over 110.

−0.667. The exponent b is also close to its expected value 0. Finally, c perfectly matches its theoretical estimate. Furthermore, we notice that the unknown constant d introduced in Eq. (24) is of the order of 1.

In brief, for the considered class of flows, we have established that, to some accuracy,

- the spectrum is Planckian,
- the temperature equals $\bar{\kappa}/2\pi$ for a width d_ξ , and
- d_ξ scales according to Eq. (24) with $d \simeq 1.6$.

These are the main results of this paper.

From our fits we also found that the broadened horizon is slightly displaced with respect to the Killing horizon by a shift $|\bar{x}_{\text{hor}}| \approx 0.1d_\xi$. However, because of the symmetry of Eq. (21), we cannot know the sign of \bar{x}_{hor} . To determine it, it is necessary to consider asymmetric flows.

IV. ASYMMETRIC FLOW PROFILES

A. Monotonic perturbations

In this section, we consider profiles of the form

$$w_{p\delta}(x) = w_p(x - \delta) - w_p(-\delta), \quad (28)$$

which are simply w_p of Eq. (6) shifted from the horizon by δ . We have subtracted the constant term so that $w_B + w_{p\delta}$ still vanishes at $x = 0$. In Fig. 8, T_0 is plotted as a function of D_p for different δ (left plot), and as a function of δ for different D_p (right plot). The behavior of these curves is quite complicated. To understand it, we first consider *smooth* perturbations, i.e. perturbations with $D_p > D_p^{\text{crit}} \approx 0.06$.

From the right panel of Fig. 8, when $D_p > D_p^{\text{crit}}$, but for both signs of δ , we see that T_0 monotonically interpolates from $T_H = \kappa_K/2\pi$, when δ is small and the perturbation is close to the horizon, to $T_B = \kappa_B/2\pi$, when $\delta \rightarrow \infty$. In that case, the perturbation is far from the horizon and thus no longer contributes to κ_K which equals its background value κ_B . When considering instead well localized perturbations, that is values of D_p smaller than D_p^{crit} , we see that T_0 oscillates, but only for δ sufficiently negative, i.e. when the perturbation is sufficiently displaced in the region where the *decaying mode* oscillates.⁶ The origin of these oscillations can be understood as follows. The scattering on the well localized bump in $\partial_x w(x)$ interferes

with the scattering on the horizon, thereby producing oscillatory behaviors.⁷

It is quite clear that the average of Eq. (20) cannot describe these oscillations. However this should *not* be conceived as limiting the validity of the observation that the temperature is given by this average. Indeed, these oscillations result from interferences between two spatially separated scatterings. In these circumstances it is meaningless to apply Eq. (20), which is based on the near horizon properties of w .

In addition, when oscillations are found for T_0 as a function of D_p or δ , the Planck character of the spectrum is *also* lost. Indeed, the parameter $\Delta_T(\omega)$ of Eq. (13) characterizing deviations from Planckianity also displays oscillations (of relative amplitude $\sim 20\%$) (see Fig. 9). As can be seen, the number of peaks increases with increasing values of $-\delta$. This is to be expected since more “room” is available to fit resonating modes. In fact this phenomenon can be viewed as a precursor of the black hole laser effect [28]. If the perturbation were strong enough to behave as a white horizon, the resonating modes would start growing exponentially [29, 30]. In that case complex-frequency modes appear when the distance between the horizons is sufficiently large, and their number increases with that distance.

To complete this analysis of the flows of Eq. (28), we verified that $\bar{\kappa}$ of Eq. (20) still approximately governs the temperature. In Fig. 10, both the numerical data (dots) and the fitted function (solid line) are reported for the series $T_0(\delta)$, with $D_p = 0.05$ and 0.15 , of Fig. 8 (right panel). This function is obtained as a two-variable function of δ and D_p by using the numerical data of T_0 . The fitting region is restricted to those values of δ for which there are no oscillations and for three values of D_p , namely $D_p = 0.05, 0.1, 0.15$. As a reference, the dotted line represents $\kappa_K(\delta)/2\pi$, i.e. the temperature one would obtain without dispersion, for $D_p = 0.05$. As a check, we also fitted the values of κ_B , κ_p and n_p and compared them with the corresponding constants used in the numerical analysis. The relative difference is very small, respectively, around 0.1%, 1% and 5%.

As one can see in Fig. 10, the agreement between the actual temperature T_0 and the average surface gravity $\bar{\kappa}/2\pi$ is quite good in the parameter region where there are no interference effects. One can also see that for $D_p = 0.05$, $\bar{\kappa}/2\pi$ of Eq. (20) follows T_0 much more closely than the surface gravity $\kappa_K(\delta)/2\pi$.

In summary, the analysis of asymmetrical perturbations first indicates that the shift \bar{x}_{hor} is always negative. That is, the broadened horizon is displaced towards the

⁶ We have adopted this formulation because, for subluminal dispersion, we expect that the sign of \bar{x}_{hor} will be the opposite, and this in virtue of the ‘symmetry’ between the behavior of modes for sub and super-luminal dispersion [14]. Indeed, for (sub) super-luminal dispersion the turning point is in the (sub) super-sonic region, see Eq. (A2). In both cases, the mode decays on the other side of the turning point [10, 12].

⁷ This is very similar to what has been found in inflation. When introducing a sharp modification of mode propagation before horizon exit, there are interferences between this localized scattering and the standard mode amplification which produce oscillations in the power spectrum, see [27] for references and a critical analysis on the generic character of this.

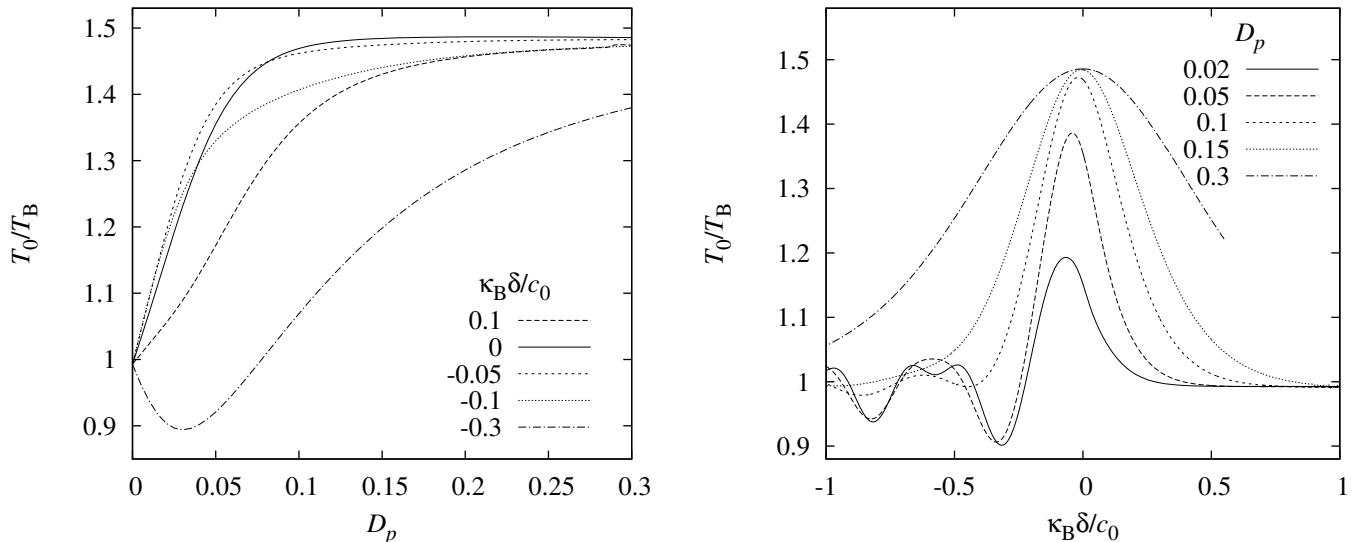


FIG. 8: On the left panel, T_0/T_B as a function of D_p for various values of δ , and, on the right, T_0/T_B as a function of δ with D_p from $D_p = 0.02$ to $D_p = 0.3$. $\Lambda/\kappa_B = 15$, $D = 0.4$, $\kappa_p/\kappa_B = 0.5$, $n = n_p = 1$. On the left panel, for values of $\delta \geq -0.05$, $T_0(D_p)$ behaves as in Fig. 6, whereas, for more negative values of δ , T_0 behaves differently. On the right panel, the asymmetry of T_0 under $\delta \rightarrow -\delta$ is clearly visible for $D_p < D_p^{\text{crit}} \approx 0.06$.

region where the decaying mode oscillates. Moreover we find that the value of the shift does not depend directly on δ . By this we mean that \bar{x}_{hor} depends on δ only because d_ξ of Eq. (24) is a function of δ through $\kappa_K(\delta)$. Second, for sufficiently smooth perturbations we found that the temperature is still approximately given by the average of Eq. (20). Finally, when the perturbation is sharp and sufficiently deep inside the supersonic region, we found that the spectrum is affected by interferences, and explained why it is so.

B. Undulations

Supersonic flows possessing a sonic horizon with a negative surface gravity κ_K behave like the time reverse of black hole horizons: long wavelength modes are blueshifted when scattered on such a horizon. Thanks to dispersion, the blueshift effect saturates, and as a result, the scattering matrix is well-defined. Moreover, for each ω , this matrix is closely related to Eq. (B8) evaluated in the corresponding black hole flow [12, 13]. In spite of this correspondence, it has been recently observed that white hole flows display a specific phenomenon related to the limit $\omega \rightarrow 0$ [15, 16]. Indeed, these flows produce a zero-frequency mode, a stationary undulation, which has a finite wavelength k_Z and a high amplitude.

To schematically describe such undulation and study its impact on the emitted spectrum, we consider the following perturbations:

$$\frac{w_p(x)}{c_0} = A \times \sin(k_Z x - \theta) \times e^{-(x/\Delta)^4}. \quad (29)$$

A is the amplitude of the undulation, and θ fixes its phase on the horizon at $x = 0$. The new length Δ is taken to be larger than $1/k_Z$, and comparable to Dc_0/κ_B which characterizes the linear regime of the background flow w_B .

In Fig. 11, T_0 is plotted versus θ for different values of k_Z , keeping fixed Ak_Z so that the surface gravity of Eq. (8) does not change with k_Z . Indeed one gets $\kappa_K(\theta) = \kappa_B + Ak_Z \cos(\theta)$. When $k_z \gg 1/d_\xi$, as expected from our previous results, the temperature is very close to $\kappa_B/2\pi$, that of the background flow w_B . Hence, independently of the value of θ , the perturbation is completely washed out by the dispersion. On the contrary, when the wavelength is larger than the width of the horizon, i.e. when $k_z < 2\pi/d_\xi \approx 30\kappa_B/c_0$, we expect that $2\pi T_0$ will be approximately given by $\kappa_K(\theta)$ given above. This can be observed for k_Z equal to $5\kappa_B/c_0$. One notices that the curve is not exactly symmetric around $\theta = \pi$. But this is also expected from the former analysis where we saw that moving the perturbation in the supersonic or in the subsonic region affects differently the spectrum.

The novelties are found for intermediate values of k_Z (say, between $10\kappa_B/c_0$ and $20\kappa_B/c_0$). For these values, $\delta_Z = 2\pi/k_Z$ is comparable to d_ξ . Hence the undulation can enter into resonance with the scattering on the horizon, thereby producing a kind of parametric amplification of the flux. This can be observed for $\theta = 0$ and $k_Z = 10\kappa_B/c_0$ where the temperature is larger than $\kappa_K/2\pi = 1.5T_B$. The fact that this resonance occurs for wavelengths $\sim d_\xi$, reinforces the fact that the effective width of the horizon is indeed d_ξ .

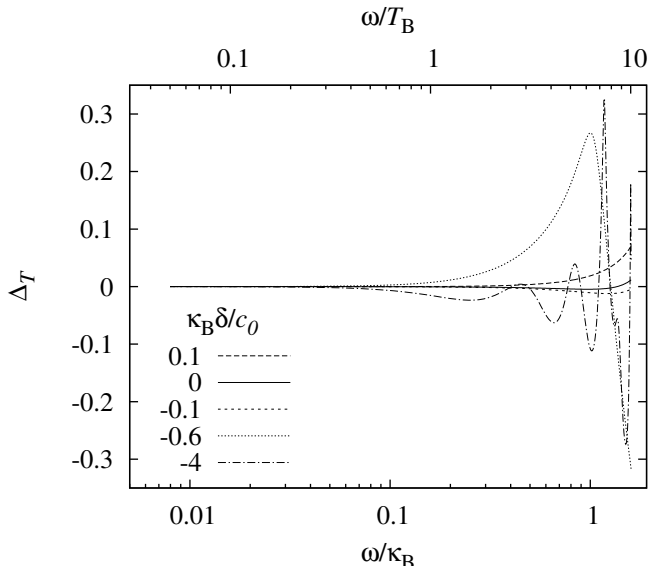


FIG. 9: The parameter $\Delta_T(\omega)$ of Eq. (13) versus ω/κ_B for different values of δ . For $\delta = 0$, continuous line, the perturbation is symmetric with respect to the horizon, and $\Delta_T(\omega)$ is extremely small in agreement with Eq. (14). When $\delta > 0$ and $(-\delta) \leq d_\xi \approx 0.2 c_0/\kappa_B$, $\Delta_T(\omega)$ stays very small and no oscillations are found. Instead when $-\delta \gg d_\xi$, oscillations of large amplitudes appear even for low frequencies, i.e. $\omega \ll \omega_{\max} \simeq 13 T_B$, thereby indicating that the spectrum is no longer Planckian. The fixed parameters are $\Lambda/\kappa_B = 15$, $D = 0.4$, $D_p = 0.02$, $\kappa_p/\kappa_B = 0.5$, $n = n_p = 1$.

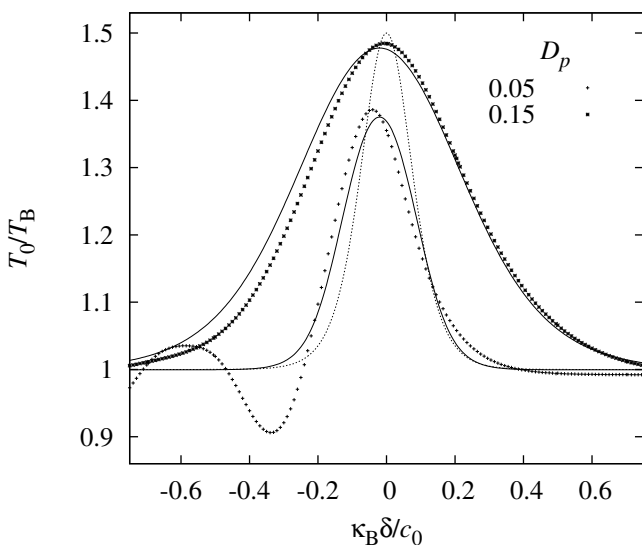


FIG. 10: Numerical data (dots) for the series $T_0(\delta)/T_B$ with $D_p = 0.15 \approx 2.5 D_p^{\text{crit}}$ and $0.05 \approx 0.8 D_p^{\text{crit}}$ of Fig. 8, right plot. The solid lines are the values of the fitted function of Eq. (20). The dotted line represents the surface gravity $\kappa_K(\delta)/2\pi$ for $D_p = 0.05$. The agreement between the temperature and $\bar{\kappa}/2\pi$ is quite good in the domains with no interference. The lowering of the peak and its shift to the left for small values of D_p are rather well reproduced. None of these effects are found when using the surface gravity $\kappa_K(\delta)$.

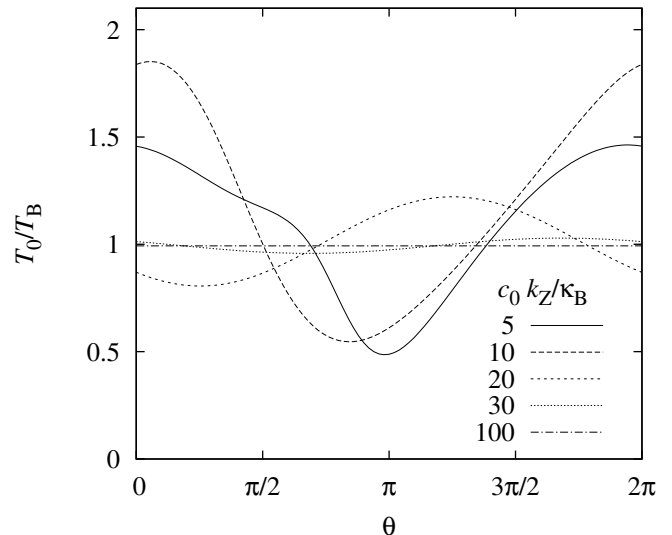


FIG. 11: T_0/T_B as a function of θ for Eq. (29), varying k_Z and A so that $A k_Z = 0.5 \kappa_B$ stays fixed. $\Delta = 2D c_0/\kappa_B$, $\Lambda/\kappa_B = 15$, $D = 0.4$, $n = 1$. For very high values of k_Z , i.e. $k_Z = 100$ and $30 \kappa_B/c_0$, the temperature is approximately $\kappa_B/2\pi$, i.e. equal to $\bar{\kappa}/2\pi$ of Eq. (20). For small values of k_Z , i.e. $k_Z = 5 \kappa_B/c_0$, T_0 also approximately follows $\bar{\kappa}(\theta)/2\pi \sim \kappa_K(\theta)/2\pi$ since the undulation wavelength is larger than d_ξ . In the intermediate regime instead, for $k_Z = 10$ and $20 \kappa_B/c_0$, the temperature widely oscillates and no longer follows $\bar{\kappa}/2\pi$.

V. CONCLUSIONS

By considering series of supersonic flows consisting on local perturbations w_p defined on the top of a background flow w_B , we were able to identify the parameters that fix the spectral properties of Bogoliubov phonons emitted by a (black hole) sonic horizon.

We show that the flux remains Planckian to a high accuracy, see Eq. (14), even when the temperature strongly differs from $T_H = \kappa_K/2\pi$, the standard value fixed by the surface gravity, see Fig. 3. This result implies two things. In spite of the fact that each mode of frequency ω has its own turning point of Eq. (A2), the Planckianity first implies that the temperature function T_ω of Eq. (11) is *not* determined by some function of $w(x)$ evaluated at a ω -dependent location, as T_ω is common to all low frequencies with respect to ω_{\max} of Eq. (A3). Second, it implies that the parameters governing the small deviations from Planckianity differ from those governing the difference between the low frequency temperature T_0 and T_H . In fact, whereas the difference $T_0 - T_H$ is governed by the *near horizon* properties, deviations from Planckianity are governed by inverse powers of ω_{\max}/T_0 , where ω_{\max} is fixed by $D_{\text{as}} = D + D_p$, characterizing the *global* properties of the supersonic transition region, such as the asymptotic velocity excess.

Moreover, in contradistinction to the relativistic case where the temperature is locally fixed by κ_K of Eq. (8),

we show that the temperature T_0 is determined, to a high accuracy when $\omega_{\max}/T_H \gtrsim 10$, by a *nonlocal* quantity: the spatial average across the horizon of $\partial_x w$ over a width d_ξ , as if the horizon were broadened.⁸ Hence, whenever $w(x)$ hardly varies over d_ξ in the near horizon region, $\bar{\kappa}$ of Eq. (20) equals the surface gravity κ_K , and the standard temperature is found. Instead, when w varies on scales shorter than d_ξ , T_0 is no longer the standard one, but it is well approximated by $\bar{\kappa}/2\pi$ for all frequencies $\omega \ll \omega_{\max}$. This result is reinforced by the fact that the effective horizon width d_ξ scales according to a well-defined law given in Eq. (24).

Furthermore, the above results are basically valid for all flows. They cease to be valid under the same restricted conditions, namely when the flow contains a sharp perturbation well localized far enough from the horizon. Then the perturbation induces a scattering that interferes with the Hawking effect, thereby engendering oscillations. These are similar to those found in inflationary spectra, and are also attributable to interferences between two scatterings. It is clear that the local average of Eq. (20) cannot describe these oscillations which are nonlocal on a scale much larger than the width d_ξ .

Hence we can conclude that when $\omega_{\max}/T_H \gtrsim 10$ and when the scattering essentially arises near the horizon, the spectrum is near Planckian, and with a temperature approximately given by $\bar{\kappa}$ of Eq. (20).

Finally, to mimic what is found in white hole flows [15, 16], we studied profiles containing an undulation on the top of a smooth profile. By varying its wavelength, we have found three different behaviors that match the above analysis.

Acknowledgments

We are grateful to Antonin Coutant and Stefano Liberati for many discussions that took place during this project. We thank Roberto Balbinot, Ted Jacobson, and Stefano Liberati for helpful comments on our manuscript. We are also grateful to Jean Macher for useful explanations concerning the code he wrote for [13].

Appendix A: Asymptotic modes and turning points

We briefly show why and how the *number* of modes of frequency ω depends on the asymptotic properties of $w = c + v$. This is important as it explains why, when there

is dispersion, there is no flux above a critical frequency ω_{\max} whose value is fixed by the asymptotic value w .

In homogeneous subsonic flows, $|v| < c$, for real ω , two roots k_ω of Eq. (9) are real, and describe the right and left moving modes. The other two roots are complex, conjugated to each other, and describe modes that are asymptotically growing or decaying, say to left. Only the first two correspond to perturbations that must be quantized, as the last two are not asymptotically bound. In infinite condensates, when canonically quantizing a field, only asymptotically bound modes (ABM) should be included in the spectrum [13, 29].

In homogeneous supersonic flows, the situation is quite different. For real ω , there exists a critical frequency ω_{\max} below which the four roots are real, as can be seen in Fig. 12 (right panel), and above which two are real and two complex, as in subsonic flows. The spectrum of ABM thus contains four modes for frequencies $0 < \omega < \omega_{\max}$ and only two for $\omega > \omega_{\max}$. At $\omega = \omega_{\max}$ the two extra roots merge and the curve $\Omega(k)$ is tangent to the line $\omega - vk$. Hence the group velocity in the lab

$$v_{\text{gr}} = \partial_k \omega = \partial_k (\Omega + vk), \quad (\text{A1})$$

vanishes at that frequency. Solving this equation one finds that ω_{\max} is proportional to Λ , but also depends also on the supersonic velocity excess $|v| - c$ (see Fig. 4 in [12] for details).

In *inhomogeneous* flows that cross once the speed of sound and with two asymptotic flat regions, i.e., as those of Eq. (5), one gets a new situation: when $\omega > \omega_{\max}$, there are still only two modes, whereas for $\omega < \omega_{\max}$, there are now three independent ABM [12]. There are only three independent modes because the semiclassical trajectories associated with the two extra roots necessarily possess a turning point for $x < 0$, in the supersonic region. Hence these two roots describe the initial and final value of the momentum of the same mode.

The location of the turning point x^{tp} depends on ω . Its value is easily obtained by solving $v_{\text{gr}} = 0$ [see Eq. (A1)]. Using Eqs. (8) and (9), for $\omega \ll \Lambda$, one finds [10]

$$- \frac{\kappa_K x^{\text{tp}}(\omega)}{c_0} \approx \left(\frac{\omega}{\Lambda} \right)^{2/3}. \quad (\text{A2})$$

For $\omega \rightarrow 0$ fixed Λ , or $\Lambda \rightarrow \infty$ fixed ω , the turning point coincides with the Killing horizon at $x = 0$, as expected from the behavior of the semiclassical trajectories in the absence of dispersion. [When considering subluminal dispersion by flipping the sign of the k^4 term in Eq. (9), one verifies that $x^{\text{tp}}(\omega)$ flips sign but keeps the same norm.]

When $\omega \rightarrow \omega_{\max}$, the turning point $x^{\text{tp}}(\omega) \rightarrow -\infty$. Hence, the threshold frequency ω_{\max} is now fixed by the *asymptotic* value of w for $x \rightarrow -\infty$. In our velocity flows of Eq. (3), one has

$$\omega_{\max} = \Lambda f(D_{\text{as}}), \quad (\text{A3})$$

where $D_{\text{as}} = -w(x = -\infty)$. Using Eqs. (5) and (6), one has $D_{\text{as}} = D + D_p$.

⁸ This is in agreement with what was found in [29] when considering the black hole laser effect [28]. In that case, the effect disappears when the distance δ_H between the black and the white horizon becomes too small, because the dispersive field is unable to ‘resolve’ the two horizons. When using linear profiles for both horizons, one finds that the critical value of $\delta_H \simeq d_\xi$.

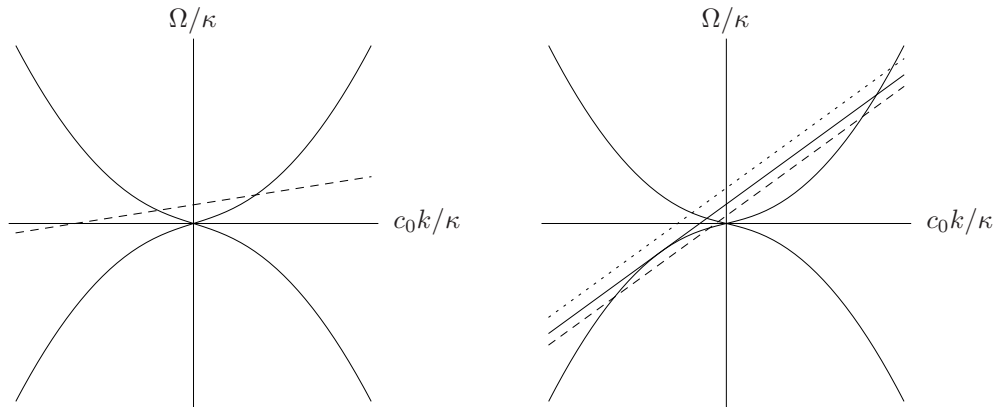


FIG. 12: Graphical solution of the dispersion relation (9) for subsonic (left panel) and supersonic flow (right panel). Solid curves: $\pm\Omega(k)/\kappa$. Left panel, dashed line: $(\omega - vk)/\kappa$. Right panel, dashed, solid, dotted lines: $\omega - vk$, respectively, for $\omega < \omega_{\max}$, $\omega = \omega_{\max}$, $\omega > \omega_{\max}$. For $\omega < \omega_{\max}$, two extra (real) roots exist in the left lower quadrant. They cease to exist for $\omega > \omega_{\max}$ and this explains why there is no Hawking radiation above ω_{\max} .

Appendix B: Mode analysis and scattering matrix

We present the main concepts that characterize the scattering of phonons in atomic Bose condensates in stationary flows containing one sonic horizon. We follow the treatment of Ref. [13] where more details can be found.

Phonon elementary excitations are described by a quantum field operator, $\hat{\phi}$. In this work, we shall use the *relative* perturbations defined by

$$\hat{\Psi} = \Psi_0(1 + \hat{\phi}), \quad (\text{B1})$$

where $\hat{\Psi}$ is the atom's field operator, and Ψ_0 the condensate. The dynamics of $\hat{\phi}$ is determined by the Bogoliubov–de Gennes equation [22]. When using $\hat{\phi}$ and when $\hbar = 1$, one obtains

$$i\partial_t \hat{\phi} = [T_\rho - iv\partial_x + mc^2] \hat{\phi} + mc^2 \hat{\phi}^\dagger, \quad (\text{B2})$$

where c is the x -dependent speed of sound

$$c^2(x) \equiv \frac{g(x)\rho_0(x)}{m}, \quad (\text{B3})$$

where $\rho_0(x) = |\Psi_0(x)|^2$ is the mean density of condensed atoms, and $g(x)$ is the effective coupling constant among atoms. These functions play no role in the sequel: only $c(x)$ and $v(x)$ matter. The quantity

$$T_\rho = -\frac{1}{2m} v \partial_x \frac{1}{v} \partial_x, \quad (\text{B4})$$

is the kinetic operator that acts on $\hat{\phi}$.

In stationary situations, $\hat{\phi}$ can be expanded in Killing frequency eigenmodes

$$\begin{aligned} \hat{\phi} &= \int d\omega \left[e^{-i\omega t} \hat{\phi}_\omega(x) + e^{+i\omega t} \hat{\phi}_\omega(x)^\dagger \right] \\ &= \int d\omega \sum_\alpha \left[e^{-i\omega t} \phi_\omega^\alpha(x) \hat{a}_\omega^\alpha + e^{+i\omega t} (\phi_\omega^\alpha(x))^* \hat{a}_\omega^{\alpha\dagger} \right], \quad (\text{B5}) \end{aligned}$$

where the discrete sum over α takes into account the number of ABM at each ω . Inserting Eq. (B5) in Eq. (B2) yields the system for the couple of modes $\phi_\omega^\alpha(x), \varphi_\omega^\alpha(x)$

$$\begin{aligned} [(\omega + iv\partial_x) - T_\rho - mc^2] \phi_\omega^\alpha(x) &= mc^2 \varphi_\omega^\alpha(x), \\ [-(\omega + iv\partial_x) - T_\rho - mc^2] \varphi_\omega^\alpha(x) &= mc^2 \phi_\omega^\alpha(x). \end{aligned} \quad (\text{B6})$$

As discussed above, in backgrounds containing one sonic horizon, they are two or three ABM depending on whether ω is larger or smaller than ω_{\max} . Therefore the ω component of the field operator reads

$$\hat{\phi}_\omega = \phi_\omega^u \hat{a}_\omega^u + \phi_\omega^v \hat{a}_\omega^v + \theta(\omega_{\max} - \omega) \varphi_{-\omega}^* \hat{a}_{-\omega}^\dagger. \quad (\text{B7})$$

The modes ϕ_ω^u and ϕ_ω^v have positive norm, they are associated with the usual real roots of Eq. (9) (see Fig. 12), and they describe, respectively, propagating right- u and left- v moving waves with respect to the condensed atoms. On the contrary, $(\varphi_{-\omega})^*$ has a negative norm. It is associated with the extra roots that exist in supersonic flows for $\omega < \omega_{\max}$, and describes phonons that are trapped inside the horizon ($x < 0$) in the supersonic region. These modes describe the negative frequency partners of the outgoing Hawking phonons represented by ϕ_ω^u and \hat{a}_ω^u .

In our infinite condensates, the above modes become superpositions of plane waves both in the left and right asymptotic regions of Eq. (B7). We can thus construct without ambiguity the in- and out-mode bases. The in modes are such that each of them contains only one asymptotic branch with group velocity directed towards the horizon. The definition of out modes is analogous and based on the criterion that each out mode contains only one asymptotic branch with group velocity directed away from the horizon.

As shown in Appendix A, for $\omega > \omega_{\max}$, there exist only two positive norm modes, and therefore in- and out-mode bases are linearly related by a trivial (elastic) 2×2 transformation. Instead, when $\omega < \omega_{\max}$, the in and out bases contain three modes which mix with each other in a

nontrivial way by a 3×3 Bogoliubov transformation [13]

$$\begin{aligned}\phi_\omega^{u,\text{in}} &= \alpha_\omega \phi_\omega^{u,\text{out}} + \beta_{-\omega} (\varphi_{-\omega}^{\text{out}})^* + \tilde{A}_\omega \phi_\omega^{v,\text{out}}, \\ (\varphi_{-\omega}^{\text{in}})^* &= \beta_\omega \phi_\omega^{u,\text{out}} + \alpha_{-\omega} (\varphi_{-\omega}^{\text{out}})^* + \tilde{B}_\omega \phi_\omega^{v,\text{out}}, \\ \phi_\omega^{v,\text{in}} &= A_\omega \phi_\omega^{u,\text{out}} + B_\omega (\varphi_{-\omega}^{\text{out}})^* + \alpha_\omega^v \phi_\omega^{v,\text{out}}.\end{aligned}\quad (\text{B8})$$

The standard normalization of the modes yields relations such as (from the first equation)

$$|\alpha_\omega|^2 - |\beta_{-\omega}|^2 + |\tilde{A}_\omega|^2 = 1. \quad (\text{B9})$$

When the initial state is vacuum, the final occupation numbers are given by the Bogoliubov coefficients

$$\begin{aligned}n_\omega &= |\beta_\omega|^2, & n_\omega^v &= |\tilde{B}_\omega|^2, \\ n_{-\omega} &= n_\omega + n_\omega^v.\end{aligned}\quad (\text{B10})$$

From these relations one sees that the norm of β_ω fixes the occupation number of outgoing phonons spontaneously produced by the scattering of the quantum field near the black hole horizon. In the standard analysis without dispersion, n_ω is Planckian and describes the Hawking effect [4]. In that case, for massless conformally invariant fields, n_ω^v , the number of left moving phonons spontaneously produced, identically vanishes. In the presence of dispersion, one generally finds $n_\omega^v \ll n_\omega$. Hence the scattering of a dispersive field on a sonic horizon basically consists of a more general and slightly modified version of the standard Hawking effect. This is true when $\omega_{\text{max}} \gtrsim 2\kappa$. For larger values of κ , the deviations become large, but the structure of Eq. (B8) and the meaning of its coefficients remain unchanged [13, 31].

-
- [1] W. G. Unruh, Phys. Rev. Lett. **46**, 1351 (1981).
 - [2] T. Jacobson, Phys. Rev. D **44**, 1731 (1991).
 - [3] T. Jacobson, Phys. Rev. D **48**, 728 (1993).
 - [4] R. Brout, S. Massar, R. Parentani, and P. Spindel, Phys. Rept. **260**, 329 (1995).
 - [5] W. G. Unruh, Phys. Rev. D **51**, 2827 (1995).
 - [6] R. Brout, S. Massar, R. Parentani, and P. Spindel, Phys. Rev. D **52**, 4559 (1995).
 - [7] S. Corley, Phys. Rev. D **57**, 6280 (1998).
 - [8] Y. Himemoto and T. Tanaka, Phys. Rev. D **61**, 064004 (2000).
 - [9] W. G. Unruh and R. Schutzhold, Phys. Rev. D **71**, 024028 (2005).
 - [10] S. Corley and T. Jacobson, Phys. Rev. D **54**, 1568 (1996).
 - [11] W. G. Unruh, PoS **QG-PH**, 039 (2007).
 - [12] J. Macher and R. Parentani, Phys. Rev. D **79**, 124008 (2009).
 - [13] J. Macher and R. Parentani, Phys. Rev. A **80**, 043601 (2009).
 - [14] A. Coutant and R. Parentani, unpublished.
 - [15] C. Mayoral, A. Recati, A. Fabbri, R. Parentani, R. Balbinot, and I. Carusotto, New J. Phys. **13**, 025007 (2011).
 - [16] S. Weinfurter, E. W. Tedford, M. C. J. Penrice, W. G. Unruh, and G. A. Lawrence, Phys. Rev. Lett. **106**, 021302 (2011).
 - [17] C. Barcelo, S. Liberati, and M. Visser, Living Rev. Rel. **8**, 12 (2005).
 - [18] J. M. Bardeen, B. Carter, and S. W. Hawking, Commun. Math. Phys. **31**, 161 (1973).
 - [19] C. W. Misner, K. S. Thorne, and J. A. Wheeler, *Gravitation* (W.H. Freeman and Co., San Francisco, 1973).
 - [20] R. Balbinot, A. Fabbri, S. Fagnocchi, and R. Parentani, Riv. Nuovo Cim. **28**, 1 (2005).
 - [21] R. Parentani, Phys. Rev. D **82**, 025008 (2010).
 - [22] F. Dalfovo, S. Giorgini, L. P. Pitaevskii, and S. Stringari, Rev. Mod. Phys. **71**, 463 (1999).
 - [23] R. Schutzhold and W. G. Unruh, Phys. Rev. D **78**, 041504 (2008).
 - [24] R. Parentani, Phys. Rev. D **63**, 041503 (2001).
 - [25] R. Parentani, Int. J. Theor. Phys. **41**, 2175 (2002).
 - [26] T. Jacobson and R. Parentani, Phys. Rev. D **76**, 024006 (2007).
 - [27] D. Campo, J. C. Niemeyer, and R. Parentani, Phys. Rev. D **76**, 023513 (2007).
 - [28] S. Corley and T. Jacobson, Phys. Rev. D **59**, 124011 (1999).
 - [29] A. Coutant and R. Parentani, Phys. Rev. D **81**, 084042 (2010).
 - [30] S. Finazzi and R. Parentani, New J. Phys. **12**, 095015 (2010).
 - [31] A. Recati, N. Pavloff, and I. Carusotto, Phys. Rev. A **80**, 043603 (2009), 0907.4305.